Decentralized Power Management of a PV/Battery Hybrid Unit in a Droop-Controlled Islanded Microgrid

Hisham Mahmood, *Member, IEEE*, Dennis Michaelson, *Member, IEEE*, and Jin Jiang, *Senior Member, IEEE*

***Abstract*—In this paper, a control strategy is proposed to achieve decentralized power management of a PV/battery hybrid unit in a droop-controlled islanded microgrid. In contrast to the common approach of controlling the PV unit as a current source, in the proposed strategy, the PV unit is controlled as a voltage source that follows a multi-segment adaptive power/frequency characteristic curve. The proposed power/frequency characteristics, of the hybrid unit and of the whole microgrid, adapt autonomously to the microgrid operating conditions so that the hybrid unit may supply the maximum PV power, match the load, and/or charge the battery, while maintaining the power balance in the microgrid and respecting the battery state-of-charge limits. These features are achieved without relying on a central management system and communications, as most of the existing algorithms do. The control strategy is implemented using multi-loop controllers, which provide smooth and autonomous transitions between the operating scenarios. Small-signal stability of the proposed control loops is investigated, and the system performance is experimentally validated on a 3.5 kVA microgrid.**

***Index Terms*—Battery storage, droop control, microgrid, PV.**

I. Introduction

FROM a control point of view, photovoltaic (PV) generation units can be classified into standalone and grid-connected configurations. Due to the intermittent nature of PV power, battery storage is employed as a critical element in PV standalone applications, to maintain the power balance in the system and enable regulation of the load voltage [1]–[4]. Islanded microgrids share the same issue with standalone systems, since the battery storage is needed to maintain the generation/load balance and to regulate the microgrid voltage and frequency. In both cases, the power management strategy should consider the state-of-charge (*SOC*) limits and the power rating of the battery.

However, unlike in standalone PV systems, in microgrids, the battery storage can be connected to the microgrid bus as a separate unit, which might be in a different location than the PV unit. Furthermore, in microgrids, the PV unit is commonly controlled as in grid-connected configurations, where the interfacing voltage sourced converter (VSC) is controlled as a current source to inject the available PV power into the grid/microgrid bus (the PQ control strategy) [5]. Since this technique was developed originally for grid-connected configurations, it does not address the power balance problem in islanded microgrids. Therefore, the operation of the PV unit, the battery storage, and other units in the microgrid, such as droop-controlled units, must be coordinated to balance the power in the islanded microgrid while respecting the battery storage limits. Accordingly, a supervisory power management strategy, which is usually implemented in a central energy management system (EMS), is required to coordinate the operation of these units [6]–[12].

The EMS in [6]–[12] requires access to the power measurements at each distributed generation (DG) unit and load node, through communication, in order to be able to maintain the power balance in the microgrid. This requires power measurement and communication modules at every generation and load node, which complicates the system and introduces potential failure modes. In all of the aforementioned strategies, communication is a critical part of the strategy. If the communication with any generation or load node is lost, the EMS may generate an undesirable control command. Therefore, dependence on communication for power management may reduce the reliability of the control strategy [13], [14]. However, communication can still be used in the grid-connected mode as a part of the tertiary control layer [15], to achieve certain objectives such as ensuring economic dispatch based on the electricity market and fuel prices. In this case, communications are not crucial to maintain the power balance in the microgrid, as it is achieved through the grid.

Moreover, in [8], the power management strategy is designed so that both the fuel cell and the battery use the droop control approach to share the peak load, when the power available from the PV unit and the microturbine is inadequate to match the load. This might deplete the battery prematurely. Instead, it is recommended that the battery only be used during transients [11], and to supply the deficit power only after the load increases beyond the total capacity of the other generating units. The EMS in [11] employs communication to ensure that the battery neither supplies nor absorbs any power at steady state. This is achieved through coordinating the power dispatched by the controllable (dispatchable) units in the microgrid.

To avoid utilizing communications, a control strategy is proposed in [16] for a microgrid composed of a PV unit and a battery storage unit. When the battery voltage exceeds its

Manuscript received September 29, 2014; revised November 28, 2014; accepted January 5, 2015. Date of publication January 20, 2015; date of current version August 21, 2015. The research work in this paper was supported by the Natural Sciences and Engineering Research Council of Canada under a Discovery Grant. The work of D. Michaelson and J. Jiang was supported by the Energy Research Initiative of the Semiconductor Research Corporation (USA). Recommended for publication by Associate Editor Y. W. Li.

The authors are with the Department of Electrical and Computer Engineering, Western University, London, ON N6A5B9, Canada (e-mail: hmahmoo2@uwo.ca; dgm@uwo.ca; jjiang@eng.uwo.ca).

Color versions of one or more of the figures in this paper are available online at http://ieeexplore.ieee.org.

Digital Object Identifier 10.1109/TPEL.2015.2394351

preset limit during charging, the battery inverter reduces the line frequency below the anti-islanding frequency limit of the PV inverter. Accordingly, the PV unit responds by disconnecting from the microgrid. The applicability of this technique is limited to microgrids where only one DG unit (battery storage) is in charge of regulating the voltage and the frequency. Hence, the technique cannot be applied to microgrids with droop-controlled units.

The PV unit is combined with the battery storage and other energy sources as a single hybrid unit in [17]–[19]. This approach is more effective since the PV controller has access to the battery *SOC* without any external communications. However, the strategy proposed in [19] requires a central controller to coordinate the operation of the hybrid unit with a diesel generator, in order to maintain the power balance in the islanded microgrid. On the other hand, the microgrids considered in [17] and [18] are composed of one hybrid source and loads, which makes the system more like a standalone power supply, rather than an islanded microgrid, from a control point of view. Therefore, these control strategies cannot be applied directly to an islanded microgrid containing multiple units, such as droop-controlled units which are widely adopted in the literature [5], [13], [14], [20]–[23].

A control strategy that employs adaptive droop control for a PV/battery hybrid unit in an islanded microgrid is investigated in [24]. This strategy exhibits a few drawbacks. First, when the PV power is very low or not available, the hybrid unit supplies power based on the maximum droop slope, which is calculated based on a predefined reduced power rating. This could deplete the battery prematurely, if the battery power rating is close or equal to the reduced power rating. Moreover, considering a steep droop slope at low PV generation can result in unstable operation. Second, in the battery charging scenario, the portion of the PV power available to charge the battery is constrained by the maximum limit of the droop slope, and the battery can only be charged by the PV power. Third, PV curtailment starts only when the battery *SOC* reaches the maximum limit. However, in practice, the charging power should be reduced gradually when the *SOC* approaches its maximum limit, to avoid battery voltage excursions.

In this paper, a decentralized power management strategy for a PV/battery hybrid unit in a droop-controlled microgrid is proposed. In the proposed strategy, the PV unit is controlled as voltage source that follows a multi-segment adaptive power/frequency characteristic curve. The proposed power/frequency characteristics, of the hybrid unit and of the whole microgrid, adapt autonomously to the operating conditions of the microgrid so that the hybrid unit may supply the maximum PV power, match the load, and/or charge the battery. This is accomplished while maintaining the power balance in the microgrid and respecting the battery SOC limits. In general, the battery module within the hybrid unit is controlled to offer the same operational functions that a separate storage unit can provide in an islanded microgrid, such as maintaining the microgrid power balance and regulating the voltage and frequency.

All these features are achieved without relying on a central management system and communications, unlike the approaches commonly proposed in the literature [6]–[12]. The control strategy is implemented using a multi-loop control, without relying on a state machine or flowcharts, which provides smoother transitions between the strategy objectives.

The objectives of the proposed control strategy and the problem statement are discussed in Section II. In Section III, the description of the islanded microgrid and the PV/battery hybrid unit is presented along with the structure of the power management strategy. The control strategy is divided into two parts, VSC control and dc–dc converters control. The VSC control system is discussed in detail in Section IV, while the dc–dc converters control system is presented in Section V. Small-signal models of the proposed control loops are developed, and stability is analyzed in Section VI. Experimental results that validate the proposed control strategy are presented and discussed in Section VII, followed by concluding remarks in Section VIII.

II. Problem Statement

The objective of the proposed control strategy is to coordinate the operation of the PV/battery unit with the other droop-controlled units, to deliver the available PV power to the microgrid, while maintaining the power balance in the system and respecting the *SOC* limits and power rating of the battery. More specifically, the proposed control strategy provides the following features without relying on communications:

1) The hybrid unit tracks and delivers all the available PV power to the microgrid after charging the battery to the desired *SOC*.
2) The hybrid unit can absorb power from the microgrid to support charging the battery without disturbing the power balance in the microgrid. In other words, the power used to charge the battery will vary autonomously based on the varying load and the available power from the PV unit to ensure that the load demand is met and to avoid exceeding the power ratings of the other units.
3) If the available PV power is more than the load demand, the hybrid unit will match the varying load while storing the surplus energy in the battery.
4) If the battery is fully charged, or if the surplus power is higher than the battery converter rating, the control strategy will autonomously adjust the PV operating point to curtail the PV power generation so that it matches the load.
5) The battery does not supply any power at steady state, unless the load increases beyond the total generation in the microgrid. Therefore, the battery within the hybrid unit can maintain the power balance in the islanded microgrid, similar to any separate battery storage unit.

The contribution of this paper is reflected in the aforementioned features, which are achieved by the proposed strategy autonomously without relying on any central management system, nor on communication, as most of the existing techniques do. This improves the reliability of the system in comparison to the strategies that employ communication and central management algorithms.

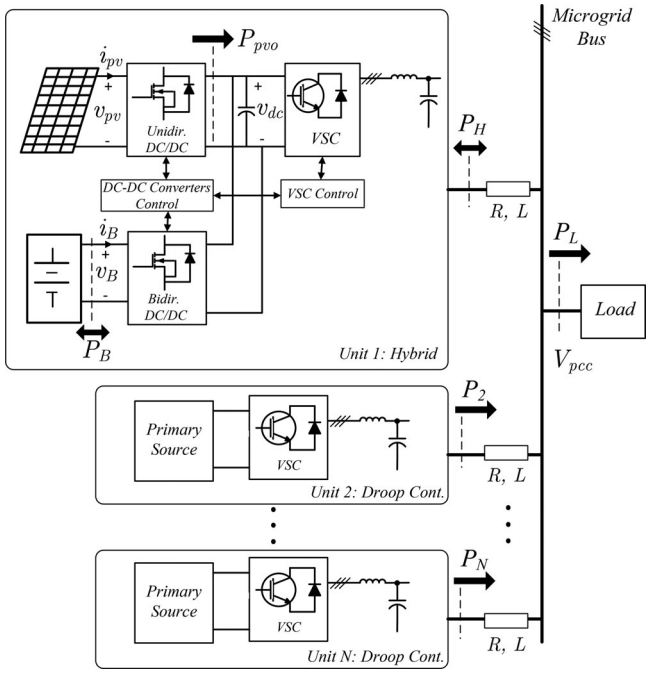

Fig. 1. Schematic diagram of the PV/battery hybrid system and the microgrid structure.

Only a single PV/battery hybrid unit is considered in this paper, as in [7]–[10], [12], [16]–[19], to introduce the concept of the proposed multi-segment adaptive P/f characteristics. The strategy can be modified to include multiple hybrid units; however, this is beyond the scope of this paper.

III. System Description and Power Management Structure

A simplified diagram of the considered microgrid structure is shown in Fig. 1. Unit 1 is the PV/battery hybrid unit under consideration, whereas Unit 2 to Unit *N* are the droop-controlled units. The block *primary source* represents a controllable (dispatchable) energy source with the required inner controllers to regulate the dc voltage at the VSC input. The PV array is interfaced to the dc-link through a unidirectional boost converter. P_{pvo} refers to the PV power injected into the dc-link. P_B represents the power at the battery terminals. The battery is interfaced with the dc-link using a bidirectional converter to ensure fully controlled charging and discharging of the battery. Also, utilizing a dc–dc converter provides flexibility in choosing the dc-link voltage level and the battery voltage and configuration [25]. In each unit, a three-phase VSC is used to interface the dc-link to the microgrid through an LC filter, an interface inductor, and a transformer. L and R represent the components of the feeders, including the interface inductor, the leakage inductance of the transformer, and the cable impedances.

The power management strategy can be subdivided into two control subsystems. The first part is the VSC control system, which is in charge of managing the power flow between the hybrid system and the microgrid. It also indirectly coordinates the operation of the PV and the battery to maintain the power balance in the hybrid system. The second is the dc–dc converters control system. This part manages the power flow among the PV array, the battery, and the dc-link in order to maintain the power balance within the hybrid system. This is achieved by controlling the dc–dc converters and the PV array voltage reference. In general, the battery dc–dc converter is controlled to regulate the dc-link voltage, while the PV converter is controlled to inject the available PV power into the dc-link.

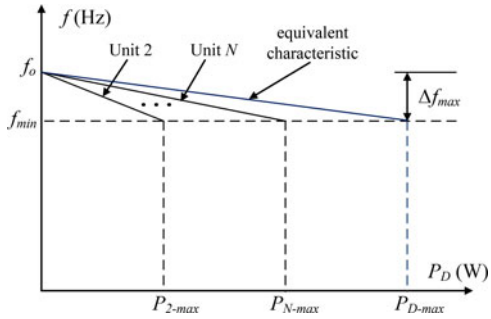

Fig. 2. Power/frequency characteristics of the droop-controlled units and the equivalent characteristic that represents the combined behavior of the units.

IV. VSC Control Strategy

The objective of the VSC control strategy is to coordinate the operation of the hybrid unit with other droop-controlled units in the microgrid. The power/frequency (P/f) characteristics of these units are illustrated in Fig. 2. The equivalent characteristic is the P/f characteristic of a single unit that represents the aggregate behavior of these droop-controlled units, with an output power of $P_D = (P_2 + \cdots + P_N)$. The power rating of the equivalent unit ($P_{D\text{-}max}$) is the sum of the power ratings of the droop-controlled units.

On the other hand, the VSC in the hybrid unit is controlled as a voltage source to regulate the unit output power (P_H) by controlling the frequency of the output voltage, as shown in Fig. 3. The output power (P_H) is indirectly regulated by controlling the battery power (P_B) using the PI controller PI_P. Since the battery dc–dc converter is maintaining the power balance within the hybrid unit by controlling the dc-link voltage, the control error (e_p) at the input of PI_P can be given by

$$\begin{aligned} e_p &= P_{B\text{-}ref} - P_B \\ &= P_{B\text{-}ref} + (P_{pvo} - P_H) \end{aligned} \tag{1}$$

where the power losses are ignored to simplify the discussion [6]–[12]. Defining P_{ref} as

$$P_{ref} = P_{B\text{-}ref} + P_{pvo} \tag{2}$$

the control error e_p can be rewritten as

$$e_p = P_{ref} - P_H\,. \tag{3}$$

Therefore, regulating P_B at $P_{B\text{-}ref}$ is equivalent to regulate the output power (P_H) at the reference P_{ref}. Note that the controller can be implemented to directly regulate P_H at the reference P_{ref}, which can be generated using the measured P_{pvo}

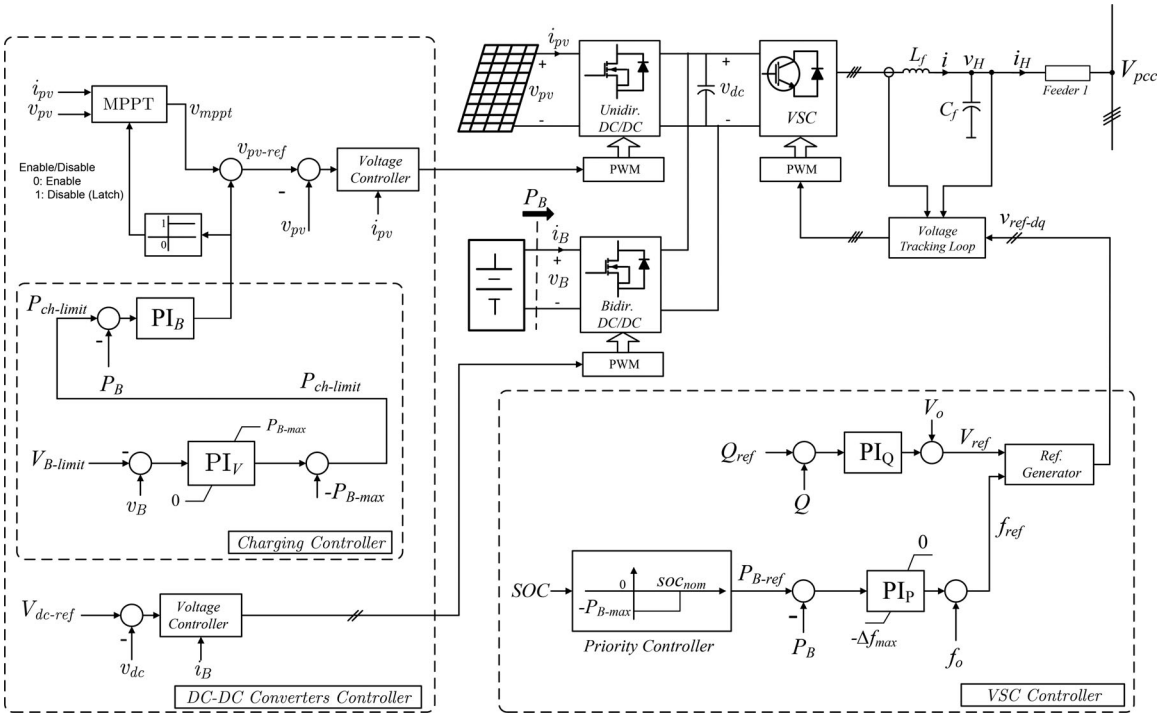

Fig. 3. Proposed control strategy.

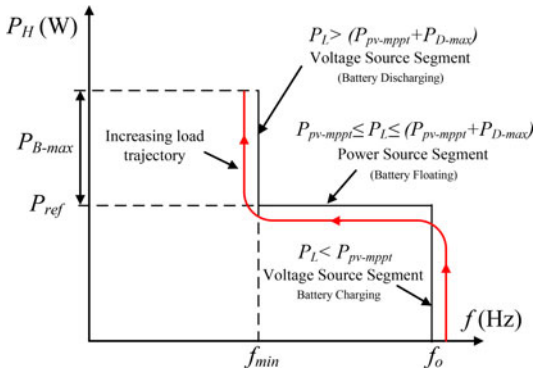

Fig. 4. Equivalent power/frequency characteristics of the hybrid unit.

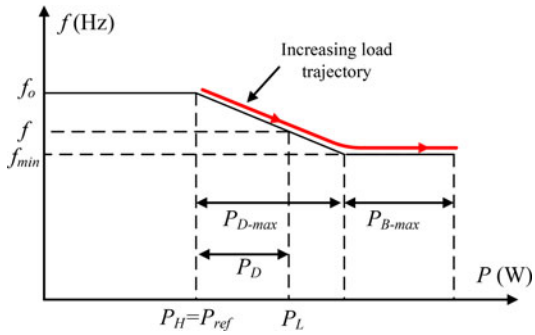

Fig. 5. Equivalent P/f characteristics of the microgrid, along with the increasing load trajectory.

and the reference $P_{B\text{-}ref}$. However, in the case of calculating the reference using the measured P_{pvo}, when the VSC output power is regulated at P_{ref}, the losses of the power converters will be supplied by the battery. Therefore, the implementation in Fig. 3 is preferred because it inherently takes into account the power converter losses.

Even though the operating frequency is used to control the power, the frequency range available to control the power is deliberately restricted within the band $[f_{min}, f_o]$ to produce the proposed P/f characteristic of the hybrid unit. The equivalent P/f characteristic of the hybrid unit, as seen by the microgrid, is illustrated in Fig. 4, where P_L is the load demand and P_{B-max} is the maximum power that can be supplied/absorbed by the battery (battery power rating). Note that since the microgrid operating frequency is regulated by the droop-controlled units based on the delivered power (P_D), the operating frequency is considered as the independent variable in Fig. 4. Despite the operating point frequency that changes with P_D, the hybrid unit regulates P_H at P_{ref}. This is achieved by using a PI controller instead of the simple proportional control (droop control) that is commonly used in grid-connected applications where the frequency is fixed by the utility grid side [26], [27]. In other words, the integral control is added to compensate for the change in frequency that is set by the droop-controlled units. To gain insight into the coordination of the microgrid units, the P/f characteristics, from Figs. 2 and 4, can be combined into one that describes the P/f characteristics of the whole microgrid, as shown in Fig. 5. The generic axis label P(W) refers to the load power in the whole microgrid, while P_L is the current load power that indicates the P/f operating point of the whole microgrid at a given instant. The shape of the P/f characteristic curve and the microgrid operating point are determined by the proposed strategy based on the variables P_L, P_{pvo}, and the battery *SOC*.

The objective of the VSC controller at any given time is either to charge the battery or to supply all the available PV power to the microgrid. The *priority controller* in Fig. 3 sets the objective of the control strategy by determining the reference $P_{B\text{-}ref}$ based on the battery SOC and the reference SOC_{nom}. The reference SOC_{nom} is the nominal SOC that the controller should always attempt to reach to ensure that the battery can support the microgrid during peak loads and/or low PV power periods. The control loops are designed so that the objective of the control strategy at any time is set based on two levels of priority as follows:

1) *Level 1:* At this level, the priority of the control strategy is either set to charge the battery or to deliver all the available PV power to the microgrid. The *priority controller* decides the objective at this level based on the battery SOC. The implementation of this controller (comparator) is discussed in Section IV-B.
2) *Level 2:* This level represents the highest priority of the control strategy, which is dedicated to maintain the power balance in the islanded microgrid, and to prevent the battery SOC and the battery power from exceeding their maximum limits, regardless of the *Level 1* priority.

The reactive power flow is controlled using a PI controller (PI_Q) to follow the reference Q_{ref} [26], [27]. The microgrid voltage is regulated by the droop-controlled units based on their V/Q droop characteristics. Therefore, the microgid bus voltage is determined by these units: the load real/reactive power demand and the feeder impedances. On the other hand, the hybrid unit regulates the reactive power by adjusting the unit output voltage so that the voltage difference across the feeder results in the desired reactive power flow (Q_{ref}). It is worth mentioning that controlling the hybrid unit as a voltage source provides the advantage of using V/Q droop control, which is commonly used in islanded microgrids [28]–[33].

To effectively explain the concept of the proposed control strategy, the microgrid operation is divided into two operating scenarios based on the battery *SOC* and the control strategy objectives. In both of these scenarios, a maximum power point tracking (MPPT) scheme is activated to track the maximum PV power ($P_{pv\text{-}mppt}$); in other words, P_{pvo}=$P_{pv\text{-}mppt}$. The details of the control action in these operating scenarios are discussed in the following sections.

A. Nominal Operating Scenario

The control strategy operates in this scenario when $SOC \geq SOC_{nom}$. Accordingly, the *priority controller* sets the reference $P_{B\text{-}ref}$ to zero, and hence, P_{ref} is determined by P_{pvo}=$P_{pv\text{-}mppt}$. Therefore, in the nominal operating scenario, the objective is to supply all available PV power to the microgrid.

It is worth emphasizing that the *priority controller* has no direct control (closed-loop control) over the battery power (P_B). Instead, the battery power is controlled indirectly by regulating the power supplied to the microgrid at the reference P_{ref}. This design allows the control strategy to place the highest priority on maintaining the power balance in the microgrid, as will be discussed later in this section. More details on direct charging control will be discussed in Section V.

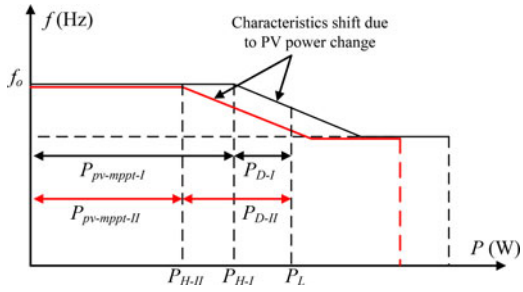

Fig. 6. P/f characteristics of the microgrid in the nominal operating scenario when the PV power decreases from $P_{pv\text{-}mppt\text{-}I}$ to $P_{pv\text{-}mppt\text{-}II}$.

The system operating point can be on any of the three P/f characteristic segments, depending on the load demand (P_L) and $P_{pv\text{-}mppt}$, as in the following three cases:

1) $P_{pv\text{-}mppt} \leq P_L \leq (P_{pv\text{-}mppt} + P_{D\text{-}max})$*:* This case corresponds to the middle segment in Figs. 4 and 5, where the hybrid unit supplies all the available PV power to the microgrid ($P_H = P_{pv\text{-}mppt}$). The rest of the load is supplied by the droop-controlled units, which cooperatively set the operating frequency according to the equivalent droop characteristics (see Fig. 2), and the supplied power P_D.

Since $P_{pv\text{-}mppt}$ depends on the solar irradiance and the temperature, the P/f characteristic in Fig. 4 may shift up or down accordingly, which corresponds to shifting the characteristic curve right or left in Fig. 5. This effect is shown in Fig. 6 where the PV power drops from $P_{pv\text{-}mppt\text{-}I}$ to $P_{pv\text{-}mppt\text{-}II}$, causing the output power to drop from $P_{H\text{-}I}$ to $P_{H\text{-}II}$, and the whole P/f characteristic to shift to the left. Accordingly, the total output power of the droop-controlled units increases from $P_{D\text{-}I}$ to $P_{D\text{-}II}$ to compensate for the reduction in PV generation, with each unit supplying its share based on its own droop characteristic (see Fig. 2).

2) $P_L > (P_{pv\text{-}mppt} + P_{D\text{-}max})$*:* The droop-controlled units reduce the frequency in response to any increase in delivered power, while the hybrid unit follows the change in frequency to maintain the output power at $P_{pv\text{-}mppt}$. The droop-controlled units reach their rated powers at $f = f_{min}$ (see Fig. 2). If the load increases and/or the PV power drops such that P_L is greater than the total of $(P_{pv\text{-}mppt} + P_{D\text{-}max})$, the droop-controlled units attempt to reduce the frequency below f_{min} according to their droop characteristics. However, according to the proposed P/f characteristic (see Fig. 5), the hybrid unit starts regulating the frequency at f_{min}. This results in regulating the output of the droop-controlled units at their rating limits and in the hybrid unit supplying the deficit in the generation/load balance while regulating the frequency at f_{min}.

This scenario corresponds to the flat segment of the P/f characteristic at f_{min} in Fig. 5, where the operating point transition into this segment is illustrated by the increasing load trajectory. The battery dc–dc converter will supply this extra power (deficit power) from the battery to maintain the dc-link voltage regulated at its nominal value. When the load decreases below $(P_{pv\text{-}mppt} + P_{D\text{-}max})$, the droop control units increase

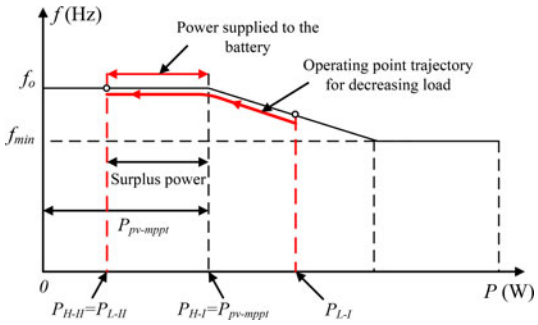

Fig. 7. P/f operating point trajectory when the load changes from $P_{L\text{-}I}$ to $P_{L\text{-}II}$, where $P_{L\text{-}II} < P_{pv\text{-}mppt}$.

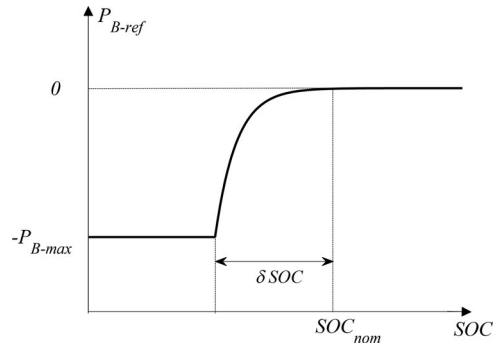

Fig. 8. $SOC/P_{B\text{-}ref}$ characteristic curve of the *priority controller*.

the frequency above f_{min}. Accordingly, the hybrid unit starts regulating the supplied power P_H at $P_{pv\text{-}mppt}$ again. It is worth mentioning that if the extra power (deficit power) increases beyond the battery power rating or the battery is fully discharged, some loads must be shed to keep the microgrid operating [5]. In this case, load shedding is inevitable, regardless of what power management strategy is used. Load shedding is considered beyond the scope of this paper.

3) $P_L < P_{pv\text{-}mppt}$*:* According to the earlier discussion, the hybrid unit always attempts to supply all available PV power $P_{pv\text{-}mppt}$ to the microgrid, while the droop-controlled units match the rest of the load. Therefore, as the load demand decreases, P_D decreases until the point when P_D reaches to zero. At this point, the entire load is being supplied by the hybrid unit ($P_H = P_{pv\text{-}mppt} = P_L$) at $f{=}f_o$. If the load decreases beyond this point, i.e., ($P_L < P_{pv\text{-}mppt}$), the droop-controlled units try to increase the frequency above f_o to avoid reverse power flow [34]. On the other hand, the hybrid unit still tries to supply $P_{pv\text{-}mppt}$ to the microgrid by increasing the frequency too. However, the upper limit of the frequency reference is set to f_o as shown in Fig. 3, and illustrated by the flat segment of the P/f characteristic at f_o in Fig. 7. This results in the hybrid unit regulating the frequency at f_o while matching the varying load demand ($P_H = P_L$) autonomously. The surplus power determined by ($P_{pv\text{-}mppt} - P_L$) tends to raise the dc-link voltage; however, since the battery dc–dc converter regulates the dc-link voltage, it will direct the surplus power to the battery. This maintains the power balance in the hybrid unit and also in the whole microgrid. This scenario is illustrated in Fig. 7 when the load drops from $P_{L\text{-}I}$ to $P_{L\text{-}II}$.

In conclusion, even though the objective is set to supply all available PV power to the microgrid, maintaining the power balance is given the highest priority, which is achieved by autonomously matching the load and storing the surplus power.

B. Battery Charging Scenario

The control strategy operates in this scenario when $SOC < SOC_{nom}$. Therefore, the reference $P_{B\text{-}ref}$ is set to $-P_{B\text{-}max}$, and accordingly, the power reference P_{ref} is set to ($P_{pvo} - P_{B\text{-}max}$). The maximum charging power is assumed to be $P_{B\text{-}max}$ in this paper; however, a different value can be used based on the battery specifications and the design preference.

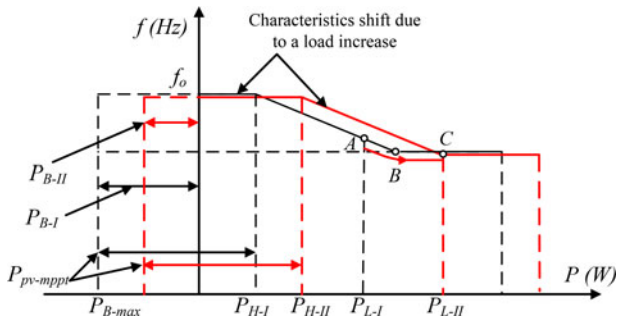

Fig. 9. P/f characteristic illustrating the *battery charging scenario* when $P_{pv\text{-}mppt} \geq P_{B\text{-}max}$, and when the load increases.

Using a hard comparator to implement the *priority controller* can result in a chattering problem in the reference $P_{B\text{-}ref}$. Instead, a fixed $SOC/P_{B\text{-}ref}$ charging curve is used as shown in Fig. 8 [35]. The $SOC/P_{B\text{-}ref}$ curve is defined by

$$P_{B\text{-}ref} = -P_{B\text{-}max} + P_{B\text{-}max}\left(1 - e^{-\frac{SOC - SOC_{nom} + \delta SOC}{\delta SOC / k_\delta}}\right) \quad (4)$$

where the constant k_δ dictates how fast the $P_{B\text{-}ref}$ curve approaches zero when the SOC approaches SOC_{nom}. Note that by choosing $\delta SOC << SOC_{nom}$, e.g., $\delta SOC{=}$ 0.1% versus $SOC_{nom}{=}$65%, the curve in Fig. 8 operates as a comparator with a soft transition in the reference $P_{B\text{-}ref}$. The behavior of the proposed control strategy in this scenario is discussed through the following two cases:

1) $P_{pv\text{-}mppt} \geq P_{B\text{-}max}$*:* In this case, the PV available power is sufficient to charge the battery at $P_{B\text{-}max}$, while the remaining power is supplied to the microgrid. The power supplied to the microgrid (P_H) is determined by the reference P_{ref}, i.e., by the difference ($P_{pv\text{-}mppt} - P_{B\text{-}max}$). When the VSC supplies this power to the microgrid, the battery dc–dc converter injects the remaining PV power ($P_{B\text{-}max}$) into the battery, to regulate the dc-link voltage. Therefore, charging the battery is indirectly achieved by controlling the power supplied to the microgrid.

Even though the objective of the control strategy during this operating scenario is to charge the battery, maintaining the power balance in the microgrid is still given the highest priority. The transition in the operating point and the P/f characteristics to maintain the power balance in the microgrid while charging the battery is illustrated in Fig. 9 and described in the following steps:

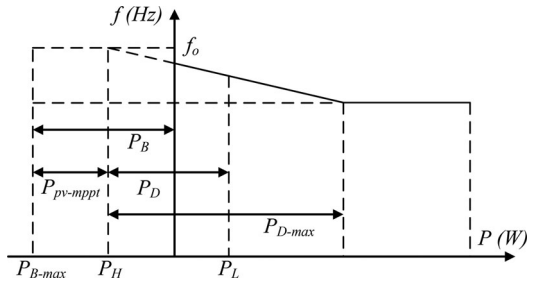

Fig. 10. P/f characteristic during the battery charging scenario when $P_{pv\text{-}mppt} < P_{B\text{-}max}$.

1) Initially, the battery is being charged solely by the PV power with $P_{B\text{-}I} = P_{B\text{-}max}$, whereas the remaining PV power is supplied to the microgrid to cover a part of the load demand $P_{L\text{-}I}$. The rest of the load is supplied by the droop-controlled units according to the equivalent droop characteristic, which determines the operating point A.
2) The droop-controlled units continue to supply any increase in the load demand until they reach their ratings at f_{min} (point B).
3) If the load increases beyond point B, e.g., to $P_{L\text{-}II}$ (point C), the droop-controlled units will attempt to decrease the operating frequency below f_{min}. However, as explained earlier, the hybrid unit starts regulating the frequency at f_{min}. This results in regulating the output of the droop-controlled units at their ratings, while the increase in the load is supplied by the hybrid unit. The increase in the hybrid unit output from $P_{H\text{-}I}$ to $P_{H\text{-}II}$ is equivalent to shifting the P/f characteristic curve to the right as shown in Fig. 9. Accordingly, the charging power is reduced by the battery dc–dc converter to $P_{B\text{-}II}$ in order to regulate the dc-link voltage.
4) The hybrid unit continues to supply any increase in the load from the PV, until it supplies all the available PV power, i.e., $P_H = P_{pv\text{-}mppt}$. In this case, the charging power is reduced to zero. Any further increase in the load demand will be met by the battery to maintain the power balance in the microgrid as in the nominal operating scenario (see Fig. 5).

In conclusion, even though the objective in this scenario is to charge the battery, the control strategy still places higher priority on maintaining the power balance in the microgrid by meeting the increasing load demand.

2) $P_{pv\text{-}mppt} < P_{B\text{-}max}$*:* In this case, P_{ref} is negative and the hybrid unit absorbs the power difference ($P_{pv\text{-}mppt} - P_{B\text{-}max}$) to support charging the battery at $P_{B\text{-}max}$. This is equivalent to shifting the P/f characteristic to the left resulting in the characteristic of Fig. 10. Under this condition, the hybrid unit is seen as a part of the load demand by the droop-controlled units.

The droop-controlled units continue to support the battery charging and supply any increase in the load until they reach their ratings. Any increase in the load beyond this point will cause the P/f characteristic to shift to the right similar to the previous case illustrated in Fig. 9.

V. DC–DC Converters Control System

In both operating scenarios discussed earlier in Section IV, the PV converter extracts and injects all the available PV power ($P_{pv\text{-}mppt}$) into the dc-link, whereas the dc-link voltage is regulated by the battery dc–dc converter. In those scenarios, the PV voltage reference ($v_{pv\text{-}ref}$) is determined solely by the MPPT algorithm.

Two operational cases have not been considered yet in the aforementioned scenarios. These cases are discussed below:

1) *Case 1:* The SOC may increase beyond the maximum preset SOC limit of the battery (SOC_{max}), while the hybrid unit is attempting to store the surplus PV power in the battery, in order to maintain the power balance in the microgrid. This may occur during the nominal operating scenario when $P_L < P_{pv\text{-}mppt}$.
2) *Case 2:* This case occurs when the surplus PV power is larger than the battery power rating $P_{B\text{-}max}$. This can only happen if the battery and its converter ratings are chosen to be less than the PV power rating. Moreover, in practice, the charging power is commonly reduced when the SOC approaches its maximum limit SOC_{max} to avoid battery voltage excursions [35], [36].

Accordingly, a dedicated controller is required to ensure controlled charging. One option is to use a simple two-stage charging control, a constant current/power stage followed by a constant voltage stage. Since the main focus of this paper is on the coordination of the hybrid unit in the microgrid, the two-stage charging is considered adequate for validating the proposed power management strategy. Moreover, the control strategy is able to incorporate different charging curves that may use the battery SOC or voltage to set the charging power reference [36]–[40].

However, since the power available to charge the battery varies based on the varying PV power and the load, the proposed controller is used here only to set the charging power limit ($P_{ch\text{-}limit}$) based on the battery voltage, as can be seen in Fig. 3. The inner P_B control loop, shown in Fig. 3, is introduced to limit the charging power from exceeding $P_{ch\text{-}limit}$ at any time.

When the voltage is lower than the set voltage limit $V_{B\text{-}limit}$, the output of the controller $\mathrm{PI_v}$ is saturated at zero, and hence, $P_{ch\text{-}limit}$ is set to $-P_{B\text{-}max}$. The controller continues operating in this constant power stage, until the battery voltage goes beyond $V_{B\text{-}limit}$. At this point, the controller $\mathrm{PI_v}$ starts reducing the charging power reference $P_{ch\text{-}limit}$ to regulate the battery voltage while charging the battery at a reduced rate.

If the charging power is less than the reference $|P_{ch\text{-}limit}|$, the output of the controller $\mathrm{PI_B}$ remains zero, and therefore, the battery continues charging at the same rate. If the load decreases and/or V_B increases such that $|P_B|$ is higher than the reference $|P_{ch\text{-}limit}|$, the controller $\mathrm{PI_B}$ starts adjusting the PV voltage so that the charging power follows the reference $P_{ch\text{-}limit}$. In other words, the charging reference sets the upper limit for the charging power.

The charging controller moves the PV operating point away from the maximum power point (MPP) (see Fig. 11), into the voltage source region of the PV characteristic curve to curtail

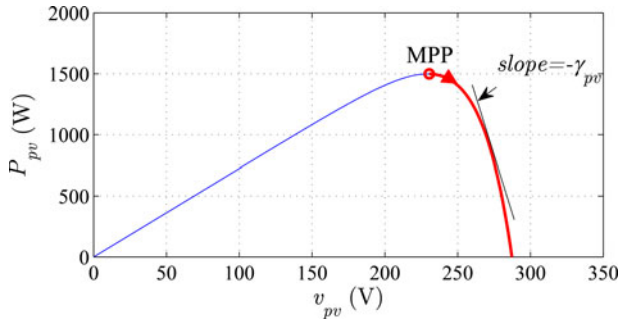

Fig. 11. PV power characteristics (Irradiance = 1000 W/m^2, T = 25 °C) showing the MPP and the PI_B control region.

the PV power until P_B settles at $P_{B\text{-}ref}$. During this control action, the MPPT algorithm is disabled and the voltage v_{mppt} is held at the most recent MPP voltage. The output of PI_B is used here to disable the MPPT scheme using the logic shown in Fig. 3.

The PI_B control loop continues adjusting the PV operating point so that the PV power autonomously matches the varying load demand and the charging power combined, as explained in the following:

1) Initially, the controller PI_B can only curtail the PV power by adjusting the PV operating point in one direction as shown in Fig. 11, which is achieved using the chosen saturation limits. Once the controller starts operating such that P_B=$P_{ch\text{-}limit}$, the PI_B output settles at a positive value due to the integral action. Accordingly, this gives the controller the freedom to adjust the operating point in both directions, reducing the PV power and, also, increasing the PV power up to the $P_{pv\text{-}mppt}$ limit.
2) If $|P_B|$ drops below $|P_{ch\text{-}limit}|$, due to an increase in demand for example, PI_B starts decreasing the PV voltage reference. This results in moving the operating point toward the MPP (increasing the PV power) until $P_B = P_{ch\text{-}limit}$ and the increase in the PV power matches the increase in the load demand. Similarly, if $|P_B|$ increases above $|P_{ch\text{-}limit}|$, the controller increases the PV voltage which moves the operating point further from the MPP. In both cases, the hybrid unit matches the change in the load demand using the PV power.

During the above control action, the hybrid unit continues operating in the same operating scenario (nominal or battery charging scenario), however with reduced PV power output.

When the load demand increases and/or the PV power drops, the controller moves the PV operating point toward the MPP until the PI_B output is reduced to zero. Consequently, the MPPT scheme is activated again, and hence, P_{pvo}=$P_{pv\text{-}mppt}$. Any increase in the load demand beyond this point will be supplied by the droop-controlled units as explained in Section IV.

VI. Small-Signal Model of the Proposed Control Loops

Modeling and control designs of the voltage controllers for the dc–dc converters and VSCs are well established in the literature. The voltage controllers for the dc–dc converter are designed in this paper as in [4], while the voltage control loops for the VSCs are designed as in [41].

Therefore, the focus of this section is only on the real/reactive control loops and the battery charging loop (P_B control loop) to gain insight into the dynamics and the control design of these loops.

A. Real/Reactive Control Loops

The real and reactive power flows at the output of the hybrid unit are described as follows [42]:

$$P_H = \frac{(RV^2 - RVV_{pcc}\cos\delta + XVV_{pcc}\sin\delta)}{R^2 + X^2} \tag{5}$$

$$Q_H = \frac{(XV^2 - XVV_{pcc}\cos\delta - RVV_{pcc}\sin\delta)}{R^2 + X^2} \tag{6}$$

where R and X are the resistive and inductive components of the feeder impedance, δ is the power angle, V is the unit output voltage, and V_{pcc} is the microgrid bus voltage. The real and reactive power controllers equations, taking into account the low-pass filters in the measurement channels, are given by

$$\omega = \omega_o + \frac{K_{p\text{-}p}s + K_{i\text{-}p}}{s}\left(P_{B\text{-}ref} - \frac{1}{Ts+1}(P_{pvo} - P_H)\right) \tag{7}$$

$$V = V_o + \frac{K_{p\text{-}q}s + K_{i\text{-}q}}{s}\left(Q_{ref} - \frac{1}{Ts+1}Q_H\right) \tag{8}$$

where V and ω are the output voltage and angular frequency, V_o and ω_o are the nominal voltage and angular frequency, $K_{p\text{-}p}$ and $K_{i\text{-}p}$ are the proportional and integral gains of the real power controller (PI_P), and $K_{p\text{-}q}$ and $K_{i\text{-}q}$ are the proportional and integral gains of the reactive power controller (PI_Q), respectively. Linearizing (5)–(8) around an operating point

$$\begin{aligned}\Delta P_H &= \left(\frac{\partial P_H}{\partial V}\right)\Delta V + \left(\frac{\partial P_H}{\partial \delta}\right)\Delta\delta \\ &= K_{pv}\Delta V + K_{p\delta}\Delta\delta\end{aligned} \tag{9}$$

$$\begin{aligned}\Delta Q_H &= \left(\frac{\partial Q_H}{\partial V}\right)\Delta V + \left(\frac{\partial Q_H}{\partial \delta}\right)\Delta\delta \\ &= K_{qv}\Delta V + K_{q\delta}\Delta\delta\end{aligned} \tag{10}$$

$$\Delta\omega = -\frac{K_{p\text{-}p}s + K_{i\text{-}p}}{s(Ts+1)}\Delta P_H \tag{11}$$

$$\Delta V = -\frac{K_{p\text{-}q}s + K_{i\text{-}q}}{s(Ts+1)}\Delta Q_H = G_v(s)\Delta Q_H \tag{12}$$

where K_{pv}, $K_{p\delta}$, K_{qv}, and $K_{q\delta}$ are evaluated at the considered operating point. Considering that $\Delta\omega = s\Delta\delta$, (11) can be rewritten as

$$\Delta\delta = -\frac{K_{p\text{-}p}s + K_{i\text{-}p}}{s^2(Ts+1)}\Delta P_H = G_\delta \Delta P_H. \tag{13}$$

TABLE I
SYSTEM PARAMETERS

Description	Parameter	Value
Nominal frequency	f_o	60 Hz
Nominal voltage (line–line)	V_o	208 V_{ll}
Hybrid unit (Unit 1) power rating	$P_{H\text{-}max}$	2500 W
Droop-controlled unit rating	$P_{D\text{-}max}$	1000 W
Frequency droop limit	Δf_{max}	0.25 Hz
Nominal dc-link voltage	$V_{\text{dc-}ref}$	400 V
Nominal battery voltage	V_B	156 V
Battery capacity	C_{bat}	32 Ah
Battery converter rating	$P_{B\text{-}max}$	1000 W
PV open-circuit voltage	V_{oc}	287 V
PV short-circuit current	I_{sc}	7.25 A
PV array power rating	$P_{pv\text{-}max}$	1.5 kW
Feeder inductance	L	4 mH
Feeder resistance	R	1.1 Ω
PI_P controller gains	$K_{p\text{-}p}$	0.0005 Hz/W
	$K_{i\text{-}p}$	0.005 Hz/(W·s)
PI_Q controller gains	$K_{p\text{-}q}$	0.01 V/var
	$K_{i\text{-}q}$	0.5 V/(var·s)
PI_B controller gains	$K_{p\text{-}B}$	0 V/W
	$K_{i\text{-}B}$	0.6022 V/(W·s)

Substituting for ΔP_H from (13) into (9), $\Delta\delta$ is given by

$$\Delta\delta = \frac{G_\delta(s)K_{pv}}{1 - K_{p\delta}G_\delta(s)}\Delta V = G_{\delta v}(s)\Delta V. \tag{14}$$

Substituting for ΔQ_H from (12) into (10), ΔV can be given by

$$\Delta V = \frac{G_v(s)K_{q\delta}}{1 - K_{qv}G_v(s)}\Delta\delta = G_{v\delta}(s)\Delta\delta. \tag{15}$$

Using (14) and (15), the characteristic equation can be written as

$$1 - G_{\delta v}(s)G_{v\delta}(s) = 0. \tag{16}$$

Substituting for $G_{\delta v}(s)$ and $G_{v\delta}(s)$ from (14) and (15), the characteristic equation can be written as follows:

$$a_5 s^5 + a_4 s^4 + a_3 s^3 + a_2 s^2 + a_1 s + a_o = 0 \tag{17}$$

where

$$a_5 = T^2 \tag{18}$$

$$a_4 = 2T + TK_{qv}K_{p\text{-}q} \tag{19}$$

$$a_3 = 1 + TK_{qv}K_{i\text{-}q} + K_{qv}K_{p\text{-}q} + TK_{p\delta}K_{p\text{-}p} \tag{20}$$

$$a_2 = K_{qv}K_{i\text{-}q} + K_{p\delta}K_{p\text{-}p} + K_{p\delta}K_{p\text{-}p}K_{qv}K_{p\text{-}q} + TK_{p\delta}K_{i\text{-}p} - K_{pv}K_{p\text{-}p}K_{q\delta}K_{p\text{-}q} \tag{21}$$

$$a_1 = K_{p\delta}K_{p\text{-}p}K_{qv}K_{i\text{-}q} + K_{p\delta}K_{i\text{-}p} + K_{p\delta}K_{i\text{-}p}K_{qv}K_{p\text{-}q} - K_{pv}K_{p\text{-}p}K_{q\delta}K_{i\text{-}q} - K_{pv}K_{i\text{-}p}K_{q\delta}K_{p\text{-}q} \tag{22}$$

$$a_0 = K_{p\delta}K_{i\text{-}p}K_{qv}K_{i\text{-}q} - K_{pv}K_{i\text{-}p}K_{q\delta}K_{i\text{-}q}. \tag{23}$$

Root trajectories considering the system parameters in Table I are shown in Fig. 12(a), when the gain $K_{i\text{-}p}$ is varied from 0.01 to 0.07 with a step of 0.005 rad/(W·s^2), and $K_{p\text{-}p} = 2\pi \times 0.0005$ rad/(W·s). The zoomed-in view of the encircled root trajectory is shown Fig. 12(b), which shows that the effect of the gain $K_{i\text{-}p}$ on the position of this pole is insignificant. The position of this pole is mainly determined by the integral gain of PI_Q.

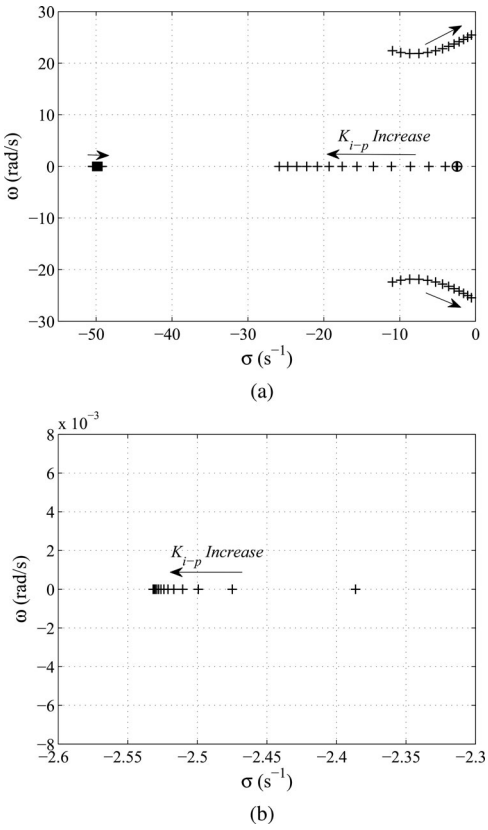

Fig. 12. Root trajectories of the real/reactive control loops when the gain $K_{i\text{-}p}$ changes from 0.01 to 0.07 with a step of 0.005 rad/(W·s^2). (a) All the roots trajectories. (b) Zoomed-in view of the least sensitive trajectory.

B. Charging Control Loop

The dynamics of the battery SOC and, hence, voltage are considerably slower in comparison to those of the control loops of the dc–dc converters and the VSC. Therefore, the set point $P_{ch\text{-}limit}$ can be considered as an independent reference.

On the other hand, the P_B control loop can be designed to have slower dynamics than those of the dc–dc converters to avoid interaction with the inner voltage control loops of these converters, which is a common practice in designing multi-loop control systems. In other words, the closed loop of the dc–dc converters can be represented as unity gains in the considered bandwidth range of the outer P_B control loop, as will be discussed next.

Accordingly, the approximated model of the P_B control loop is developed as shown in Fig. 13(a). The transfer functions G_{pv} and G_B represent the dynamics of the PV and the battery control loops, while $f(v_{pv})$ represents the P_{pv}/v_{pv} characteristic curve (see Fig. 11), which is a nonlinear function. This function can be approximated by a straight line in the PV characteristic region under consideration as illustrated in Fig. 11, where $-\gamma_{pv}$ indicates the slope of the line. Considering the linearized PV characteristic curve and that G_{pv} and G_B are approximated by unity

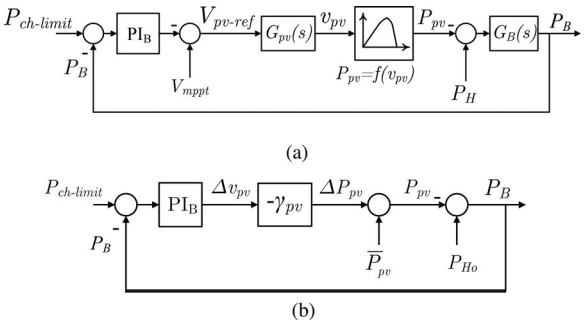

Fig. 13. Approximated model of the P_B Control Loop. (a) Nonlinear model. (b) Linearized model.

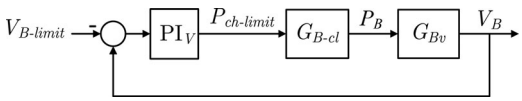

Fig. 14. Approximated model of the charging control loop.

gains in the loop bandwidth under consideration, the linearized model of the charging loop is illustrated in Fig. 13(b). $\overline{P}_{pv}$ and P_{Ho} represent the PV power and the load power, supplied by the hybrid unit, at the considered operating point. Accordingly, the open-loop transfer function can be given by

$$G_{B\text{-}ol} = \frac{K_{p\text{-}B}\,s + K_{i\text{-}B}}{s}\gamma_{pv} \tag{24}$$

where $K_{p\text{-}B}$ and $K_{i\text{-}B}$ are the proportional and integral gains of the controller PI$_B$. By setting $K_{p\text{-}B}=0$, the closed-loop results in a first-order transfer function as follows:

$$G_{B\text{-}cl} = \frac{1}{T_{ch}\,s+1} \tag{25}$$

where

$$T_{ch} = \frac{1}{K_{i\text{-}B}\gamma_{pv}}. \tag{26}$$

In conclusion, a simple integral controller can be used in the charging control loop. The gain $K_{i\text{-}B}$ is chosen so that the P_B control loop is 10–15 times slower than the inner control loops. The voltage control loops (inner loops) are designed as in [4], which results in closed loop crossover frequencies of 271 and 471 rad/s for the battery and the PV controllers, respectively. Considering the nominal PV characteristics in Fig. 11, $\gamma_{pv} \approx 40$ W/V around $\overline{P}_{pv} = 1000$ W. Accordingly, choosing $K_{i\text{-}B}$ as 0.6775 results in $1/T_{ch} = 27.1$ rad/s, which is one-tenth of the bandwidth of the slowest inner loop (271 rad/s).

Consequently, the outer voltage control loop can be modeled as in Fig. 14. The transfer function G_{Bv} is used to describe the behavior of the battery voltage around the maximum voltage limit ($V_{B\text{-}limit}$) operating region. To gain insight into the behavior of the battery in this operating region, the experimental results in Fig. 15 show the battery voltage excursions beyond the maximum limit $V_{B\text{-}limit}$ of 185 V, when the battery is being charged at a constant rate (P_{Bo}) of 780 W at high SOC levels ($SOC > 90\%$).

The battery voltage behavior can be approximated by two lines in the considered operating region as shown in Fig. 15.

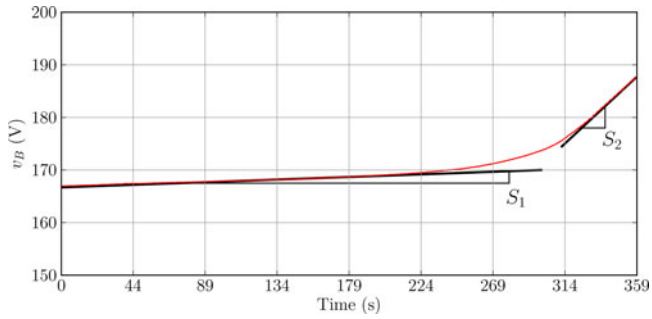

Fig. 15. Experimental results illustrating the battery voltage excursion beyond $V_{B\text{-}limit}$ during unconstrained constant power charging.

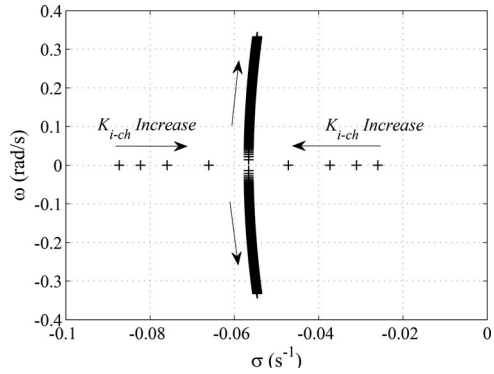

Fig. 16. Dominant root trajectories of the charging control loop when the gain K_{i-ch} is varied from 2 to 100 with a step of 0.25.

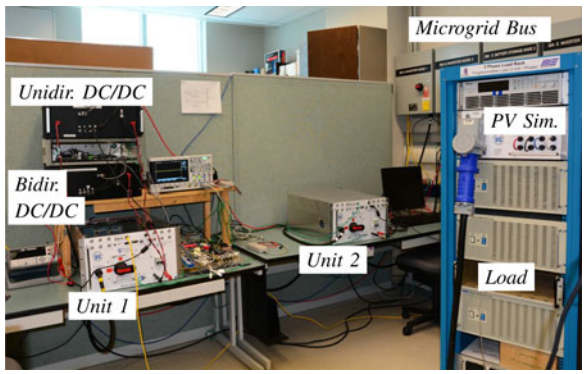

Fig. 17. Experimental microgrid prototype.

Accordingly, the transfer function G_{Bv} can be approximated by an integrator as below

$$G_{Bv} = \frac{K_{Bv}}{s} \tag{27}$$

where the constant K_{Bv} has two different values which correspond to the different operating segments represented by the slopes S_1 and S_2. Considering the battery voltage behavior in Fig. 15, K_{Bv} can be approximated by two values, $K_{Bv1} = 5.38 \times 10^{-5}$ V/(W·s) and $K_{Bv2} = 1.129 \times 10^{-3}$ V/(W·s), corresponding to S_1/P_{Bo} and S_2/P_{Bo}.

Note that when the charging power changes, the slopes S_1 and S_2 will change, since they represent the change in voltage versus time (V/s) at a certain charging power. However, the gains K_{Bv1} and K_{Bv2} can still approximate the battery behavior since

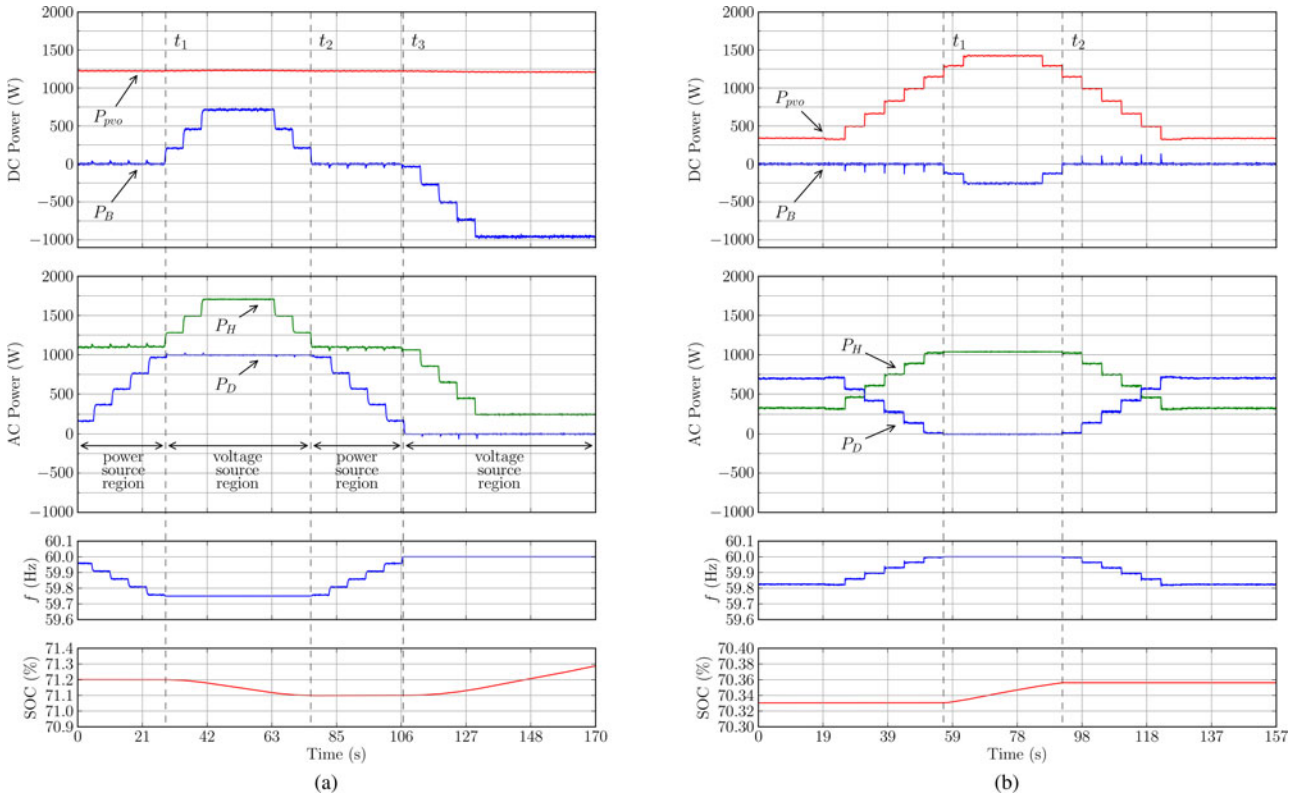

Fig. 18. Experimental performance of the proposed strategy during the nominal operating scenario: (a) In response to load changes, and (b) in response to PV power changes.

they represent the change in voltage versus charging power and time V/(W·s). For a more accurate approximation, a specific set of charging curves can be used to calculate the gains K_{Bv1} and K_{Bv2} for a specific set of charging rates.

From Fig. 14, the characteristic equation of the closed-loop system is given by

$$T_{ch}s^3 + s^2 + K_{p\text{-}ch}K_{Bv}s + K_{i\text{-}ch}K_{Bv} = 0. \qquad (28)$$

Considering that $K_{Bv} = K_{Bv2}$ and $K_{p\text{-}ch} = 100$, while varying $K_{i\text{-}ch}$ from 2 to 100 with a step of 0.25, the dominant root trajectories are shown in Fig. 16.

VII. Experimental Validation

A. Experimental Setup

The power management strategy is validated experimentally on a two-unit prototype microgrid that is shown in Fig. 17. Unit 1 is the hybrid unit, while Unit 2 represents the equivalent of the droop-controlled units with a combined output power of P_D. The droop-controlled unit is powered by a Chroma 62050H dc power supply. The PV array is emulated using a commercial PV simulator from Chroma. Both units are connected to a three-phase microgrid bus, which is connected to a programmable load bank. The key parameters of the experimental system are shown in Table I. The hybrid unit is configured as in Fig. 1 with MOSFET-based boost and synchronous boost topologies used for the unidirectional and bidirectional converters, respectively. The inverters are based on six-switch IGBT modules. The control strategy is programmed to run on the Texas Instruments TMS320F28335 floating-point microcontrollers that control the power electronic converters. The experimental data collection programs are written in Python and run on a Ubuntu Linux platform, which is connected to the microcontrollers using Texas Instruments Ethernet-to-serial converters.

B. Experimental Results

The performance of the proposed strategy is validated through experiments under the nominal scenario with changes in both load and generation, and under the charging scenario. Additional experiments show the transition between the scenarios and the action of the charging control loop.

1) Nominal Scenario: Performance of the proposed strategy during the nominal operating scenario in response to load changes is illustrated in Fig. 18(a). During this scenario, the SOC is higher than SOC_{nom}, which is set to 65%. To effectively illustrate the performance, the system behavior is divided into four regions.

Between $t = 0$ and $t = t_1$, the hybrid unit delivers all available PV power to the microgrid by regulating the battery power at $P_B = 0$ W. Therefore, the hybrid unit appears in the microgrid as a power-controlled source. On the other hand, the increasing load demand is met by the droop-controlled unit. This results in dropping the frequency in response to the increasing load. The

droop-controlled unit continues to supply the increasing load demand until it reaches its maximum power rating of 1000 W at $t = t_1$. At this point, the frequency reaches its minimum limit of f_{min}, i.e., 59.75 Hz.

From $t = t_1$ to $t = t_2$, the load increases beyond the power available from the PV and the droop-controlled unit, combined ($P_L > P_{pv\text{-}mppt} + P_{D\text{-}max}$). As discussed in Section IV-A and illustrated by the microgrid P/f characteristics (see Fig. 5), the hybrid unit starts regulating the operating frequency at f_{min}, which results in limiting the P_D at $P_{D\text{-}max}$. Consequently, the hybrid unit operates as a voltage source and, therefore, matches the varying load by supplying the deficit power from the battery, resulting in a drop in the SOC.

At $t = t_2$, the load demand drops below the total of ($P_{pv\text{-}mppt} + P_{D\text{-}max}$), and therefore, the hybrid unit returns to operating as a power-controlled source, while the droop-controlled unit supplies the rest of the load.

The load demand continues to drop until $P_D = 0$ W at $t = t_3$. For $t \geq t_3$, the load decreases below the available PV power, i.e., $P_L < P_{pv\text{-}mppt}$. Consequently, as discussed in Section IV-A (see Fig. 7), the hybrid unit autonomously starts acting as a voltage source, while regulating the frequency at $f = f_o$ and matching the available load demand in the microgrid. As can be seen in Fig. 18(a), the surplus power from the PV is absorbed by the battery to maintain the power balance in the hybrid unit and, also, in the microgrid.

Performance of the strategy in response to PV power changes is illustrated in Fig. 18(b). In this experiment, the load is kept constant around 1000 W, and the PV power is varied by changing the irradiance setting in the PV simulator from 200 to 1000 W/m^2.

Between $t = 0$ and $t = t_1$, it is shown in Fig. 18(b) that the hybrid unit tracks and supplies all the available PV power to the microgrid while regulating the battery power at $P_{B\text{-}ref} = 0$ W, as explained in Section IV-A. Since the load demand is kept constant, the output power from the droop-controlled unit is reduced in response to the increasing power from the hybrid unit, which operates as a power controlled source in this period. The output power P_H continues to increase with increasing PV power until it supplies all the load, and P_D reduces to zero.

The increase in the PV power beyond this limit (for $t \geq t_1$) results in the controller PI_P (see Fig. 3) saturating at $f = f_o$. This causes the hybrid unit to behave as a voltage source and, therefore, matches the load demand. This shows how the highest priority of maintaining the power balance in the microgrid is achieved by the control strategy autonomously. Consequently, the surplus PV power is absorbed by the battery, which is responsible for regulating the dc-link voltage and, hence, maintaining the power balance within the hybrid unit. The battery continues to store the surplus energy until the PV power drops below the load demand.

Moreover, the performance of the control strategy in response to both load and PV power changes is illustrated in Fig. 19. As in the previous experiments, Fig. 19 shows the effective response of the strategy to variations in load and PV power. The hybrid unit successfully maintains the power balance in the microgrid, by supplying the deficit power in the microgrid for $t \leq t_1$ and $t \geq t_4$, and absorbing the surplus power between $t = t_2$ and $t = t_3$.

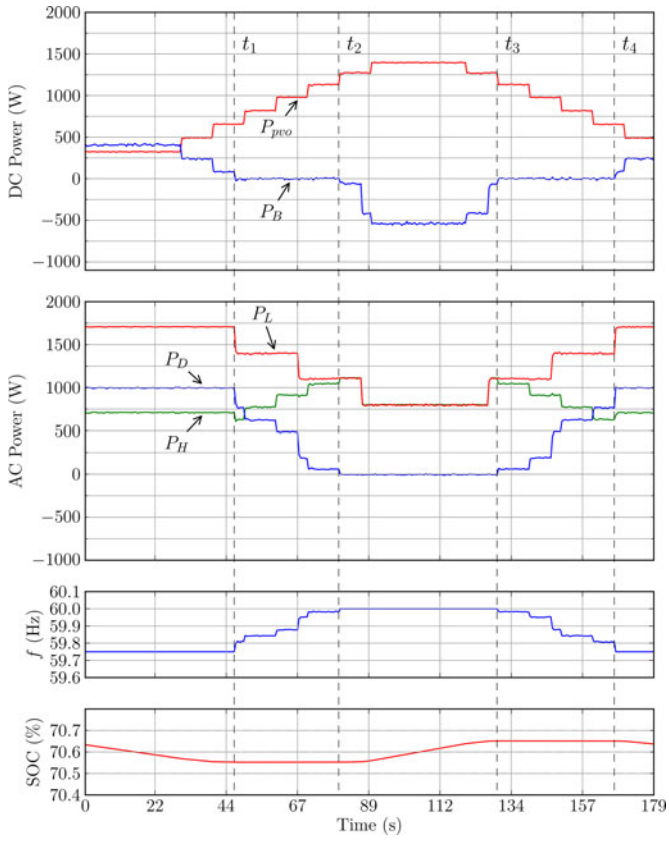

Fig. 19. Experimental performance during the nominal operating scenario in response to both PV and load demand variations.

2) Charging Scenario: The performance of the proposed strategy during the charging operating scenario is illustrated in Fig. 20. In this scenario, the objective is to charge the battery at $P_{B\text{-}max}$ (-1000 W). Since the available PV power is less than $P_{B\text{-}max}$, the rest of the charging power and the losses are imported from the microgrid. In this case, the hybrid unit appears as a load in the microgrid, which is equivalent to shifting the P/f characteristic to the left as explained in Section IV-B (see Fig. 10).

When the load starts increasing at $t = t_1$, the droop-controlled unit starts supplying the increased load demand, while the battery is still being charged at its maximum rating until P_D reaches $P_{D\text{-}max}$ at $t = t_2$. As the load increases beyond this point, the hybrid unit starts regulating the frequency at f_{min}, due to the chosen limit of the controller PI_P output. This results in limiting the output of the droop-controlled units at their rated powers while reducing the power flow into the hybrid unit until $P_H = 0$ W. This happens because the hybrid unit operates as a voltage-controlled source that regulates the frequency. On the other hand, the output powers of the droop-controlled units are regulated at their ratings, i.e., they start operating as power-controlled sources.

Any increase in the load demand beyond this point will be supplied by the hybrid unit as the P/f characteristic continues to shift to the right until all the PV power is being delivered

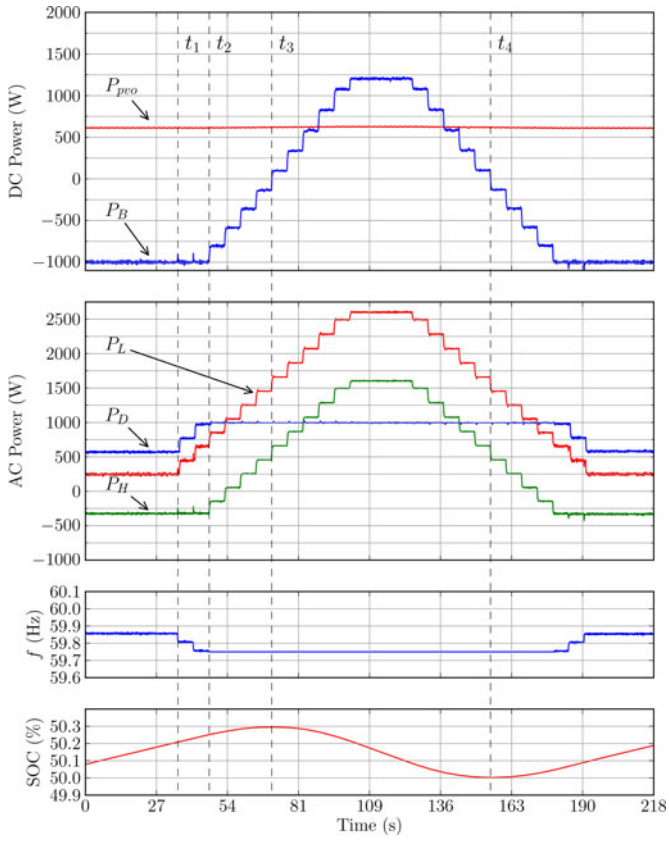

Fig. 20. Experimental results of the proposed strategy during the charging operating scenario.

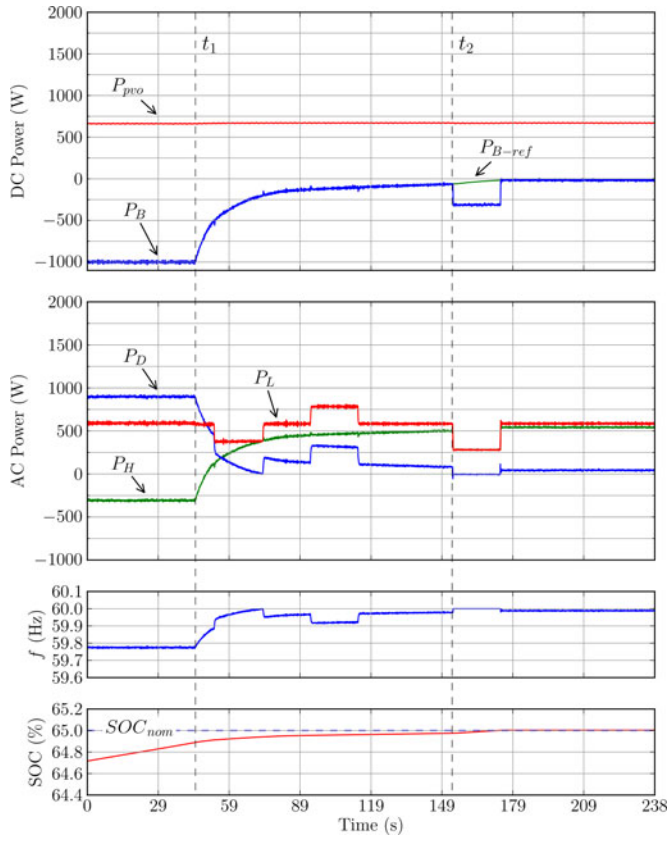

Fig. 21. Experimental results of the proposed strategy during transition from the charging scenario to the nominal operating scenario.

to the load, which happens at $t = t_3$. At this moment, the P/f characteristic curve will resemble the one in Fig. 5. Any further increase in the load will be supplied by the battery as discussed in Section IV-A.

The control strategy resumes charging the battery after the load demand drops below the total generation as shown in Fig. 20 for $t > t_4$.

3) Transition Between Operating Scenarios: The performance of the proposed strategy during a transition from the charging scenario to the nominal operating scenario is illustrated in Fig. 21. In this experiment, δSOC is set to 0.1%, while SOC_{nom} is set to 65%.

Initially, the system is operating in the charging scenario while the battery is being charged at its maximum rating. The SOC continues increasing until it reaches the limit of $(SOC_{nom} - \delta SOC)$, i.e., 64.9% at $t = t_1$. At this moment, the charging priority controller starts reducing the reference $P_{B\text{-}ref}$ exponentially as a function of the rising SOC (see Fig. 8). As can be seen in Fig. 21, the charging power is reduced and, consequently, the hybrid unit output P_H increases until all the available PV power is delivered to the microgrid.

Moreover, the load P_L is stepped up and down several times to examine the performance of the power control loop during the transition phase, in response to load disturbances. As shown in Fig. 21, the hybrid unit continues to operate as a power-controlled source until $t = t_2$. At this point, the load demand is dropped below the supplied PV power, and therefore, the hybrid unit autonomously starts to operate as a voltage source to match the available load demand while regulating the frequency at f_o.

4) Performance of the Charging Control Loop: The performance of the battery voltage and charging control loops is validated through experiments. The results are shown in Fig. 22. Initially, the load is less than 200 W, while the available PV power is 1000 W, which forces the hybrid unit to operate as a voltage source to match the available load demand. In this case, the battery is used to store the surplus PV power in order to maintain the power balance in the microgrid. The battery is being charged continuously until a voltage excursion occurs at $t = t_1$, when the voltage starts to exceed the maximum voltage limit of the battery $V_{B\text{-}limit}$. This indicates that the battery can no longer be charged at the current rate.

Accordingly, the controller PI_V (see Fig. 3) starts reducing the charging limit reference $P_{ch\text{-}limit}$ at $t = t_1$. Once the charging limit reference becomes less than charging power P_B, the controller PI_B starts reducing the PV power output so that P_B matches $P_{ch\text{-}limit}$. As shown in Fig. 22, the control loop disables the MPPT algorithm and starts increasing the PV voltage to move the PV operating point to the right of the MPP on the PV curve.

To examine the performance of the proposed strategy in the event of load changes, the load is stepped up and down several times starting at $t = t_2$. The results show that the control strategy can successfully adjust the PV operating point autonomously so that the PV power matches the varying load while regulating the

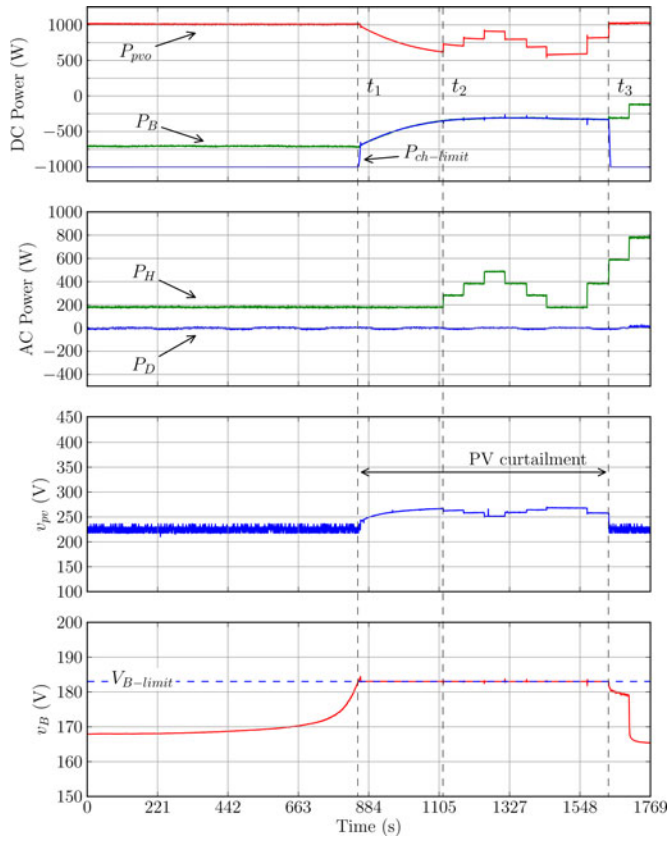

Fig. 22. Experimental results showing the action of the proposed charging controller.

battery voltage at its limit. At $t = t_3$, the load demand increase forces the PV operating point to move back to the MPP while enabling the MPPT algorithm again.

VIII. Conclusion

In this paper, a power management strategy that enables controlling a PV/battery unit as a voltage source in an islanded microgrid is proposed. In contrast to the common approach of controlling the PV unit as a current source in the literature, it is shown that controlling the hybrid unit as a voltage source that follows the proposed adaptive power/frequency characteristics can achieve decentralized control of the hybrid unit in the islanded microgrid without relying on a central EMS and communications. It is demonstrated experimentally that the proposed power/frequency characteristics can adapt autonomously to the microgrid operating conditions so that the hybrid unit may supply the maximum PV power, match the load, and/or charge the battery, while maintaining the power balance in the microgrid and respecting the battery *SOC* limits. Also, small-signal stability of the proposed control loops is investigated to gain insight into the dynamics of these loops.

References

[1] S. J. Chiang, H.-J. Shieh, and M.-C. Chen, "Modeling and control of a PV charger system with SEPIC converter," vol. 56, no. 11, pp. 4344–4353, Nov. 2009.

[2] F. Locment, M. Sechilariu, and I. Houssamo, "DC load and batteries control limitations for photovoltaic systems. Experimental validation," *IEEE Trans. Power Electron.*, vol. 27, no. 9, pp. 4030–4038, Sep. 2012.

[3] F. Ongaro, S. Saggini, and P. Mattavelli, "Li-ion battery-supercapacitor hybrid storage system for a long lifetime, photovoltaic-based wirless sensor network," *IEEE Trans. Power Electron.*, vol. 27, no. 9, pp. 3944–3952, Sep. 2012.

[4] H. Mahmood, D. Michaelson, and J. Jiang, "Control strategy for a standalone PV/battery hybrid system," in *Proc. IEEE Ind. Electron. Conf.*, 2012, pp. 3412–3418.

[5] J. A. P. Lopes, C. L. Moreira, and A. G. Madureira, "Defining control strategies for microgrids islanded operation," *IEEE Trans. Power Syst.*, vol. 21, no. 2, pp. 439–449, May 2006.

[6] C. Wang and M. H. Nehrir, "Power management of a stand-alone wind/photovoltaic/fuel cell energy system," *IEEE Trans. Energy Convers.*, vol. 23, no. 3, pp. 957–967, Sep. 2008.

[7] B. Belvedere, M. Bianchi, A. Borghetti, C. A. Nucci, M. Paolone, and A. Peretto, "A microcontroller-based power management system for a standalone microgrids with hybrid power supply," *IEEE Trans. Sustainable Energy*, vol. 3, no. 3, pp. 422–431, Jul. 2012.

[8] K. T. Tan, X. Y. Peng, P. L. So, Y. C. Chu, and M. Z. Q. Chen, "Centralized control for parallel operation of distributed generation inverters in microgrids," *IEEE Trans. Smart Grid*, vol. 3, no. 4, pp. 1977–1987, Dec. 2012.

[9] B. Wang, M. Sechilariu, and F. Locment, "Intelligent DC microgrid with smart grid communications: Control strategy consideration and control," *IEEE Trans. Smart Grid*, vol. 3, no. 4, pp. 2148–2156, Dec. 2012.

[10] K. T. Tan, P. L. So, Y. C. Chu, and M. Z. Q. Chen, "Coordinated control and energy management of distributed generation inverters in microgrid," *IEEE Trans. Power Del.*, vol. 28, no. 2, pp. 704–713, Apr. 2013.

[11] J. Kim, J. Jeon, S. Kim, C. Cho, J. Park, H. Kim, and K. Nam, "Cooperative control strategy of energy storage system and microsources for stabilizing the microgrid during islanded operation," *IEEE Trans. Power Electron.*, vol. 25, no. 12, pp. 3037–3048, Dec. 2010.

[12] Y.-K. Chen, Y.-C. Wu, C.-C. Song, and Y.-S. Chen, "Design and implementation of energy management system with fuzzy control for dc microgrid systems," *IEEE Trans. Power Electron.*, vol. 28, no. 4, pp. 1563–1570, Apr. 2013.

[13] K. Brabandere, B. Bolsens, J. V. Keybus, A. Woyte, J. Driesen, and R. Belmans, "A voltage and frequency droop control method for parallel inverters," *IEEE Trans. Power Electron.*, vol. 22, no. 4, pp. 1107–1115, Jul. 2007.

[14] R. H. Lasseter, J. H. Eto, B. Schenkman, J. Stevens, H. Vollkommer, D. Klapp, E. Linton, H. Hurtado, and J. Roy, "CERTS microgrid laboratory test bed," *IEEE Trans. Power Del.*, vol. 26, no. 1, pp. 325–332, Jan. 2011.

[15] J. M. Guerrero, J. C. Vasquez, J. Matas, L. G. de Vicuña, and M. Castilla, "Hierarchical control of droop-controlled ac and dc microgrids—A general approach towards standardization," *IEEE Trans. Ind. Electron.*, vol. 58, no. 1, pp. 158–172, Jan. 2011.

[16] E. Serban and H. Serban, "A control strategy for a distributed power generation microgrid application with voltage- and current controlled source converter," *IEEE Trans. Power Electron.*, vol. 25, no. 12, pp. 2981–2992, Dec. 2010.

[17] S. Bae and A. Kwasinski, "Dynamic modeling and operation strategy for a microgrid with wind and photovoltaic resources," *IEEE Trans. Smart Grid*, vol. 3, no. 4, pp. 1867–1876, Dec. 2014.

[18] L. Valverde, F. Rosa, and C. Bordons, "Design, planning and management of a hydrogen-based microgrid," *IEEE Trans. Ind. Informat.*, vol. 9, no. 3, pp. 1398–1404, Aug. 2013.

[19] S. Adhikari and F. Li, "Coordinated V-f and P-Q control of solar photovoltaic generators with MPPT and battery storage in microgrids," *IEEE Trans. Smart Grid*, vol. 5, no. 3, pp. 1270–1281, May 2014.

[20] C. N. Rowe, T. J. Summers, R. E. Betz, D. J. Cornforth, and T. G. Moore, "Arctan power–frequency droop for improved microgrid stability," *IEEE Trans. Power Electron.*, vol. 28, no. 8, pp. 3747–3759, Aug. 2013.

[21] M. Savaghebi, A. Jalilian, J. C. Vasquez, and J. M. Guerrero, "Autonomous voltage unbalance compensation in an islanded droop-controlled microgrid," *IEEE Trans. Ind. Electron.*, vol. 60, no. 4, pp. 1390–1402, Apr. 2013.

[22] I. U. Nutkani, P. C. Loh, and F. Blaabjerg, "Droop scheme with considering of operating cost," *IEEE Trans. Power Electron.*, vol. 29, no. 3, pp. 1047–1052, Mar. 2014.

[23] D. De and V. Ramanarayanan, "Decentralized parallel operation of inverters sharing unbalanced and nonlinear loads," *IEEE Trans. Power Electron.*, vol. 25, no. 12, pp. 3015–3025, Dec. 2010.

[24] H. Mahmood, D. Michaelson, and J. Jiang, "A power management strategy for PV/battery hybrid systems in islanded microgrids," *IEEE J. Emerging Sel. Topics Power Electron.*, vol. 2, no. 4, pp. 870–882, Dec. 2014.
[25] W. Jiang, and B. Fahimi, "Active current sharing and source management in fuel cell-battery hybrid power system," vol. 57, no. 2, pp. 752–761, Feb. 2010.
[26] J. Kim, J. Guerrero, P. Rodriguez, R. Teodorescu, and K. Nam, "Mode adaptive droop control with virtual output impedances for an inverter-based flexible AC microgrid," *IEEE Trans. Power Electron.*, vol. 26, no. 3, pp. 689–700, Mar. 2011.
[27] M. Dai, M. N. Marwali, J.-W. Jung, and A. Keyhani, "Power flow control of a single distributed generation unit," *IEEE Trans. Power Electron.*, vol. 23, no. 1, pp. 343–352, Jan. 2008.
[28] W. Yao, M. Chen, J. Matas, J. M. Guerrero, and Z.-M. Qian, "Design and analysis of the droop control method for parallel inverters considering the impact of the complex impedance on the power sharing," *IEEE Trans. Ind. Electron.*, vol. 58, no. 2, pp. 576–588, Feb. 2011.
[29] Y. W. Li and C.-N. Kao, "An accurate power control strategy for power-electronics-interfaced distributed generation units operating in a low-voltage multibus microgrid," *IEEE Trans. Power Electron.*, vol. 24, no. 12, pp. 2977–2988, Dec. 2009.
[30] Q.-C. Zhong, "Robust droop controller for accurate proportional load sharing among inverters operated in parallel," *IEEE Trans. Ind. Electron.*, vol. 60, no. 4, pp. 1281–1290, Apr. 2013.
[31] J. He and Y. W. Li, "An enhanced microgrid load demand sharing strategy," *IEEE Trans. Power Electron.*, vol. 27, no. 9, pp. 3984–3995, Sep. 2012.
[32] J. He, Y. W. Li, J. M. Guerrero, F. Blaabjerg, and J. C. Vasquez, "An islanding microgrid power sharing approach using enhanced virtual impedance control scheme," *IEEE Trans. Power Electron.*, vol. 28, no. 11, pp. 5272–5282, Nov. 2013.
[33] Y. Zhang and H. Ma, "Theoretical and experimental investigation of networked control for parallel operation of inverters," *IEEE Trans.Ind. Electron.*, vol. 59, no. 4, pp. 1961–1970, Apr. 2012.
[34] R. H. Lasseter and P. Piagi, "Control and design of microgrid components, final project report," Power System Engineering Research Center, University of Wisconsin, Madison, WI, USA, Tech. Rep. 06-03, Jan. 2006.
[35] P. Thounthong, S. Rael, and B. Davat, "Control algorithm of fuel cell and batteries for distributed generation system," *IEEE Trans. Energy Convers.*, vol. 23, no. 1, pp. 148–155, Mar. 2008.
[36] E. Koutroulis and K. Kalaitzakis, "Novel battery charging regulation system for photovoltaic applications," *IEE Proc. Electr. Power Appl.*, vol. 151, no. 2, pp. 191–197, Mar. 2004.
[37] Y. Cao, S. Tang, C. Li, P. Zhang, Y. Tan, Z. Zhang, and J. Li, "An optimized EV charging model considering TOU price and SOC curve," *IEEE Trans. Smart Grid*, vol. 3, no. 1, pp. 388–393, Mar. 2012.
[38] H. Fakham, D. Lu, and B. Francois, "Power control design of a battery charger in a hybrid active PV generator for load-following applications," *IEEE Trans.Ind.Electron.*, vol. 58, no. 1, pp. 85–94, Jan. 2011.
[39] Z. Miao, L. Xu, V. R. Disfani, and L. Fam, "An SOC-based battery management system for microgrids," *IEEE Trans. Smart Grid*, vol. 5, no. 2, pp. 966–973, Mar. 2014.
[40] R. F. Nelson, "Power requirements for batteries in hybrid electric vehicles," *J. Power Sources*, vol. 91, no. 1, pp. 2–26, Aug. 2000.
[41] M. B. Delghavi and A. Yazdani, "A control strategy for islanded operation of a distributed resource (DR) unit," in *Proc. IEEE Power Energy Soc. Gen. Meet.*, 2009, pp. 1–8.
[42] E. A. A. Coelho, P. C. Cortizo, and P. F. D. Garcia, "Small signal stability for single phase inverter connected to a stiff AC system," in *Proc. IEEE 34th Ind. Appl. Conf.*, 1999, pp. 2180–2187.

Hisham Mahmood (S'10–M'15) received the M.E.Sc. degree in control engineering from Lakehead University, Thunder Bay, ON, Canada, in 2008, and the Ph.D. degree in electrical engineering from the University of Western Ontario, London, ON, in 2014.

He is currently a Postdoctoral Fellow with the Department of Electrical and Computer Engineering, University of Western Ontario. His research interests include modeling and control of switching power converters, distributed generation, renewable energy interface, microgrids, and power quality.

Dennis Michaelson (M'12) received the B.A.Sc. degree in automation engineering from Simon Fraser University, Burnaby, BC, Canada, in 1993. He is currently working toward the Ph.D. degree with the Department of Electrical and Computer Engineering, Western University, London, ON, Canada.

He previously held the position of Vice-President of Engineering for EK3 Technologies, Inc., where he led a team developing networked embedded systems for multimedia applications. His research interests include control of energy storage in microgrids, power electronic converters, mobile robotics, and embedded real-time systems.

Jin Jiang (S'85–M'87–SM'94) received the Ph.D. degree from the University of New Brunswick, Saint John, NB, Canada, in 1989.

Since 1991, he has been with the Department of Electrical and Computer Engineering, Western University, London, ON, Canada, where he is currently a Senior Industrial Research Chair Professor. He also works closely with the International Atomic Energy Agency on modern control and instrumentation for nuclear power plants. His research interests include fault-tolerant control of safety-critical systems, advanced control of electrical power plants, and power systems involving renewable energy resources.

Dr. Jiang is a Fellow of Canadian Academy of Engineering. He is also a Member of the International Electrotechnical Commission 45A subcommittee to develop industrial standards on instrumentation and control for nuclear facilities.